Nonlinear Dyn (2019) 98:1049–1063
https://doi.org/10.1007/s11071-019-05248-3

ORIGINAL PAPER

Dynamic analysis of a simplified flexible manipulator with interval joint clearances and random material properties

Dongyang Sun · Baoqiang Zhang · Xuefeng Liang · Yan Shi · Bin Suo

Received: 3 January 2019 / Accepted: 8 September 2019 / Published online: 16 September 2019

Abstract Flexible manipulator is an emerging technique in aerospace engineering, especially in the assembly, testing and maintenance of space stations. Dynamic analysis of a flexible manipulator with multiple clearance joints and hybrid uncertainties is a great challenge as compared to traditional flexible manipulator. To solve the problem, a dynamics model for a simplified flexible manipulator with interval clearance joints and random material properties was established. In this model, the Lankarani–Nikravesh contact force model was used to construct the clearance joint, while a combined feedforward–feedback control strategy based on a PID controller was applied to control the flexible manipulator. In addition, the clearance sizes and the Young's moduli of the flexible parts were described by interval variables and random fields, respectively. To solve the dynamics model, a general methodology, based on the Karhunen–Loève expansion and Kriging model, was presented. Finally, numerical examples were employed to demonstrate the validity of the proposed approach. The simulation results indicate that the joint clearance, the flexibility of the components and the uncertainties have great impacts on the kinematic accuracy and dynamic behaviors of the flexible manipulator, while hybrid uncertainties result in worse kinematic accuracy and more complex dynamic behaviors.

Keywords Interval uncertainty · Random field · Flexible manipulator · Clearance · Karhunen–Loève expansion

Dongyang Sun and Baoqiang Zhang have contributed equally to this work.

D. Sun (✉) · X. Liang
College of Aerospace Engineering, Chongqing University, Chongqing 400044, China
e-mail: dongyangsunnuaa@gmail.com

B. Zhang
School of Aerospace Engineering, Xiamen University, Xiamen 361005, China

Y. Shi
State Key Laboratory of Mechanics and Control of Mechanical Structures, Nanjing University of Aeronautics and Astronautics, Nanjing 210016, China

B. Suo
Institute of Electronic Engineering, CAEP, Mianyang 621900, China

1 Introduction

With the development of space technologies, large and lightweight flexible manipulators have been widely used to assemble, mend and test space station, capture spacecraft, finish extravehicular work of the astronaut, etc. The reliabilities of the manipulator are crucial to the space missions. The dynamic analysis of the flexible manipulator involves solving the problems of clearance impact during the working process and the uncertainties of the structure parameters. In order to improve the accuracy of dynamic analysis, these factors should be carefully considered and analyzed.

In the past decades, researchers have focused on the studies of clearance joint. Flores et al. [1] have systematically demonstrated the dynamic behaviors of planar and spatial rigid mechanisms with dry clearance joints or lubricated clearance joints. The simulation results illustrated that the clearance affects the dynamic performance of the mechanisms and reduces the kinematic accuracy. Meanwhile, lubricants can eliminate the influence of the clearance on the dynamic behaviors and kinematic accuracy of the mechanisms. Erkaya [2] presented a dynamic model for a welding robot manipulator with clearance joint. Varedi et al. [3,4] investigated the effects of joint clearances on the dynamic behaviors of a 3-RRR parallel manipulator, and presented a method based on the particle swarm optimization to reduce these influences. Considering the existing of multiple clearance joints, Bai and Sun [5], and Ma and Qian [6] investigated the dynamic behaviors of planar mechanisms with multiple revolute clearance joints. From the simulation results, they conclude that multiple clearance joints lead to worse dynamic behaviors of the mechanisms. Zhang et al. [7] developed an analytical procedure for dynamic analysis of a 3-PRR parallel mechanism with multiple clearance joints. For the flexible model, Abdallah et al. [8] investigated the dynamic behaviors of flexible planar slider-crank mechanisms with multiple clearance joints. The results showed that the flexibility of the components plays an important role in the dynamic performance of the mechanisms with clearance joints. Li et al. [9] established a dynamics model for a large-scale flexible solar array system with clearance joints and analyzed the effects of the clearance on the dynamic performance of the system. Tian et al. [10] investigated the effects of lubricated cylindrical joint on dynamic behaviors of a flexible spatial multibody system with large deformation, established based on the absolute nodal coordinate formulation (ANCF).

The aforementioned studies mainly focused on the dynamic analysis of manipulators with deterministic parameters. However, the widely existing uncertainties, such as material imperfection, machining errors and abrasion, cannot be neglected. Uncertainties are usually classified to random uncertainty and epistemic uncertainty, respectively. Probability theory is provided for the representation of the random uncertainty, while evidence theory, possibility theory, interval analysis and fuzzy set theory are introduced to represent the epistemic uncertainty [11,12]. Chaker et al. [13] presented a methodology, based on a stochastic method, for kinematic accuracy analysis of a 3-RCC spherical parallel manipulator with clearance and manufacturing errors. The simulation results show that the clearance and manufacturing errors have impacts on the kinematic accuracy of the manipulator, and the comprehensive influence cannot be obtained by the linear combination of the effects of the clearance and manufacturing errors. It is concluded that, for a manipulator with clearance and manufacturing errors, these two factors should be considered in the modeling process. Pandey and Zhang [14] analyzed the reliability of a robotic manipulator with random clearance joints based on the principle of maximum entropy. Li et al. [15] investigated the kinematic accuracy and dynamic behaviors of a two-link rigid manipulator with clearance joints and random parameters. Sun [16] established a model for kinematic accuracy analysis of a flexible manipulator with an interval clearance joint. Yan and Guo [17] also investigated the other mechanisms with clearance joint and uncertainty.

The dynamics of a manipulator with random and epistemic uncertainties is complex. Wang et al. [18] are among the few researchers who investigated the dynamic performance of a 3-RRS flexible parallel manipulator with hybrid uncertain parameters based on the ANCF and Chebyshev method. Sun et al. [19] investigated the dynamic behaviors of a planar mechanism with random parameters and an interval clearance joint. In the previous studies, the inhomogeneous distribution of the materials has not been considered. However, the inhomogeneity will result in continuous uncertainties of the material properties. Thus, in many cases, uncertain fields are used to describe the uncertainty of the material properties. Wu et al. [20,21] investigated the dynamic behaviors of flexible mechanisms and rigid–flexible mechanisms with random uncertainty. In their work, the flexible mechanism is constructed based on the ANCF, while random fields are applied to represent the uncertainty of the material properties. To our knowledge, no investigations have been conducted on the dynamic behaviors of a flexible manipulator with hybrid uncertainties and considering the inhomogeneous distribution of the material properties in space. For a flexible manipulator with hybrid uncertainties and uncertain fields, there exist three challenges. First, an appropriate mathematical model should be selected to represent each uncertainty. Second, the influences of each uncertainty on the results should be analyzed separately. Third, due to low com-

puting efficiency of uncertainty analysis of a flexible manipulator with hybrid uncertainties, surrogate model needs to be constructed in the uncertainty analysis. However, the last step has not been reported for a flexible manipulator with hybrid uncertainties and uncertain fields. To solve this problem, we investigated the kinematic accuracy and dynamic behaviors of a simplified flexible manipulator with interval clearance joints and random fields, and developed a methodology, based on the Karhunen–Loève expansion and Kriging model, for dynamic analysis of a flexible manipulator with interval uncertainty and random fields. Finally, the validity and feasibility of these methods are demonstrated.

2 Modeling of the simplified flexible manipulator with clearance joints

2.1 Joint clearance model

A revolute clearance joint, as shown in Fig. 1, consisted of two parts: bearing and journal. The bearing and journal were fixed to the body i and body j, respectively. XY is the global coordinate system. Points P_i and P_j are the centers of the bearing and journal, respectively. $\mathbf{r}_i$ and $\mathbf{r}_j$ are the position vectors of points P_i and P_j, respectively. The eccentricity vector between the two points is expressed as

$$\mathbf{e}_{ij} = \mathbf{r}_j - \mathbf{r}_i \tag{1}$$

The unit eccentricity vector is given by

$$\mathbf{n} = \frac{\mathbf{e}_{ij}}{e_{ij}} \tag{2}$$

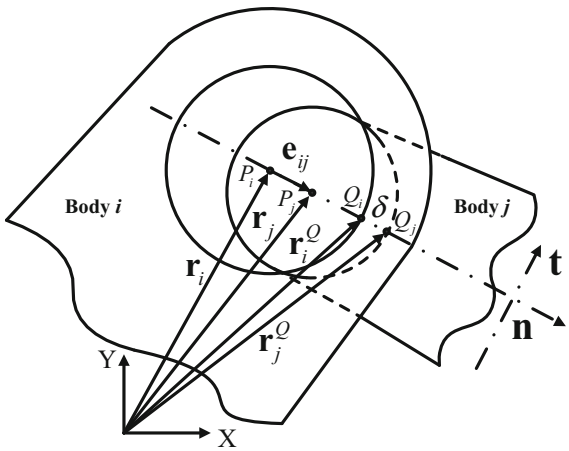

Fig. 1 The model of the revolute clearance joint

where e_{ij} is the magnitude of the eccentricity vector. When the bearing and journal contact, the relative penetration depth (δ) can be expressed as

$$\delta = e_{ij} - c \tag{3}$$

where c is the radial clearance size, $c = R_i - R_j$. R_i and R_j are the radii of the bearing and journal, respectively.

Based on the ANCF, the position vectors of the contact points on body i and j are expressed as

$$\mathbf{r}_k^Q = \mathbf{r}_k + R_k\mathbf{n} \quad (k = i, j) \tag{4}$$

The velocity vectors of the contact points can be evaluated by differentiating Eq. (4) with respect to time, yielding

$$\dot{\mathbf{r}}_k^Q = \dot{\mathbf{r}}_k + R_k\dot{\mathbf{n}} \quad (k = i, j) \tag{5}$$

The relative scalar velocities, normal and tangential to the plane of collision, are expressed as

$$v_{\mathrm{N}} = \left(\dot{\mathbf{r}}_j^Q - \dot{\mathbf{r}}_i^Q\right)^{\mathrm{T}}\mathbf{n} \tag{6}$$

$$v_{\mathrm{T}} = \left(\dot{\mathbf{r}}_j^Q - \dot{\mathbf{r}}_i^Q\right)^{\mathrm{T}}\mathbf{t} \tag{7}$$

where the tangent vector $\mathbf{t}$ can be obtained by rotating vector $\mathbf{n}$ by 90° counterclockwise.

2.2 Mathematical formula of the simplified flexible manipulator with clearance joints

A simplified flexible manipulator with clearance joints is shown in Fig. 2, in which the joints O and A are imperfect joints, respectively. τ_1 and τ_2 represent control torques, acting on joints O and A, respectively.

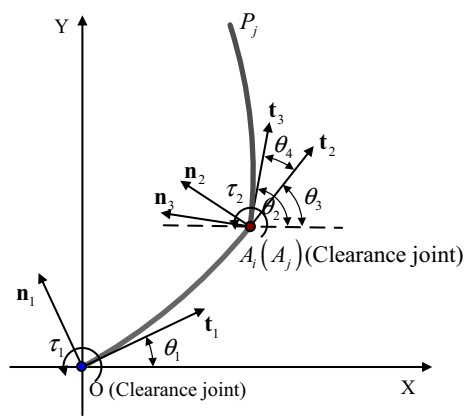

Fig. 2 Simplified flexible manipulator with clearance joints

$\mathbf{n}_1-\mathbf{t}_1$, $\mathbf{n}_2-\mathbf{t}_2$ and $\mathbf{n}_3-\mathbf{t}_3$ are local coordinate systems at points O, A_i and A_j, respectively. θ_1 and θ_3 denote the angles of link OA_i at points O and A_i, respectively. θ_2 is the angle of link A_jP_j at points A_j. To describe the large deformation of the flexible manipulator, the ANCF was applied to construct the dynamic model of the manipulator.

In the ANCF, the global position vector of a point on a beam element is expressed as [22]

$$\mathbf{r} = \mathbf{S}\mathbf{e}^k \tag{8}$$

where $\mathbf{S}$ is the global element shape function associated with $x(x \in [0\ l])$, which is given by,

$$\begin{aligned}
&\mathbf{S} = \begin{bmatrix} S_1\mathbf{I}_2 & S_2\mathbf{I}_2 & S_3\mathbf{I}_2 & S_4\mathbf{I}_2 \end{bmatrix} \qquad (9)\\
&S_1 = 1 - 3\left(\frac{x}{l}\right)^2 + 2\left(\frac{x}{l}\right)^3,\\
&S_2 = l\left[\frac{x}{l} - 2\left(\frac{x}{l}\right)^2 + \left(\frac{x}{l}\right)^3\right],\\
&S_3 = 3\left(\frac{x}{l}\right)^2 - 2\left(\frac{x}{l}\right)^3,\\
&S_4 = l\left[\left(\frac{x}{l}\right)^3 - \left(\frac{x}{l}\right)^2\right] \qquad (10)
\end{aligned}$$

where $\mathbf{I}_2$ is the unit matrix of size 2. l is the initial length of the beam element. The nodal coordinate vector, $\mathbf{e}^k$, has the form of

$$\mathbf{e}^k = \left[\mathbf{r}_m^{\mathrm{T}} \left(\frac{\partial \mathbf{r}_m}{\partial x}\right)^{\mathrm{T}} \mathbf{r}_n^{\mathrm{T}} \left(\frac{\partial \mathbf{r}_n}{\partial x}\right)^{\mathrm{T}}\right]^{\mathrm{T}} \tag{11}$$

where $\mathbf{r}_i$ and $\partial \mathbf{r}_i/\partial x$ are the global displacement and the global slope of node i $(i = m, n)$, respectively. Based on the description above, the kinetic energy of the beam element is calculated by

$$T_{\mathrm{e}} = \frac{1}{2}\int_V \rho \dot{\mathbf{r}}^{\mathrm{T}}\dot{\mathbf{r}}\mathrm{d}V = \frac{1}{2}\left(\dot{\mathbf{e}}^k\right)^{\mathrm{T}}\mathbf{M}_{\mathrm{e}}\dot{\mathbf{e}}^k \tag{12}$$

where V and ρ are the volume and density of the beam element, respectively. $\mathbf{M}_{\mathrm{e}}$ is the constant mass matrix of the element, which is obtained by

$$\mathbf{M}_{\mathrm{e}} = \frac{1}{2}\int_V \rho \mathbf{S}^{\mathrm{T}}\mathbf{S}\mathrm{d}V \tag{13}$$

The strain energy of the beam element is evaluated as

$$U_{\mathrm{e}} = \frac{1}{2}\int_V \boldsymbol{\sigma}^{\mathrm{T}}\boldsymbol{\varepsilon}\mathrm{d}V \tag{14}$$

where $\boldsymbol{\varepsilon}$ and $\boldsymbol{\sigma}$ are the strain and stress vectors, respectively.

The virtual work of the control torques is expressed as

$$\delta W = \tau_1\delta\theta_1 + \tau_2\delta\theta_4 = \tau_1\delta\theta_1 + \tau_2\delta\theta_2 - \tau_2\delta\theta_3 \tag{15}$$

where $\delta\theta_1$ can be expressed by the global slope of node O, $\left[\partial r^1_{ox}/\partial x\ \ \partial r^1_{oy}/\partial x\right]^{\mathrm{T}}$, as follows

$$\delta\theta_1 = \frac{\partial r^i_{ox}/\partial x\delta\left(\partial r^i_{oy}/\partial x\right) - \partial r^i_{oy}/\partial x\delta\left(\partial r^i_{ox}/\partial x\right)}{f_1^2} \tag{16}$$

where $f_1 = \sqrt{\left(\partial r^1_{ox}/\partial x\right)^2 + \left(\partial r^1_{oy}/\partial x\right)^2}$. The equivalent generalized force for control torque τ_1 is expressed as

$$\mathbf{Q}_1 = \left[0\ 0\ -\tau_1\left(\partial r^1_{oy}/\partial x\right)/f_1{}^2\ \ \tau_1\left(\partial r^1_{ox}/\partial x\right)/f_1^2\ 0\ 0\ 0\ 0\right]^{\mathrm{T}} \tag{17}$$

Similarly, the equivalent generalized force for control torque τ_2 also can be obtained. Based on the principle of the virtual work and Baumgarte method, the dynamics equation of the flexible manipulator with clearance joints is expressed as

$$\begin{bmatrix} \mathbf{M} & \boldsymbol{\Phi}_{\mathbf{q}}^{\mathrm{T}} \\ \boldsymbol{\Phi}_{\mathbf{q}} & \mathbf{0} \end{bmatrix}\begin{bmatrix} \ddot{\mathbf{q}} \\ \boldsymbol{\lambda} \end{bmatrix} = \begin{bmatrix} \mathbf{B}\boldsymbol{\tau} - \mathbf{F} + \mathbf{F}_c \\ \boldsymbol{\gamma} - 2\alpha\dot{\boldsymbol{\Phi}} - \beta^2\boldsymbol{\Phi} \end{bmatrix} \tag{18}$$

where $\mathbf{M}$ is the constant mass matrix of the manipulator, $\boldsymbol{\lambda}$ denotes the Lagrange multiplier vector, $\mathbf{F}$ is the generalized elastic force, $\mathbf{F}_c$ is the generalized contact force, $\boldsymbol{\Phi}$ and $\boldsymbol{\Phi}_{\mathbf{q}}$ represent the constraint equation and its Jacobian matrix with respect to the generalized coordinate vector $\mathbf{q}$, respectively, α and β are the Baumgarte parameters, $\boldsymbol{\gamma} = -\left(\boldsymbol{\Phi}_{\mathbf{q}}\dot{\mathbf{q}}\right)_{\mathbf{q}} - 2\boldsymbol{\Phi}_{\mathbf{q}t}\dot{\mathbf{q}} - \boldsymbol{\Phi}_{tt}$, and $\mathbf{B}\boldsymbol{\tau}$ is the generalized control torque. $\boldsymbol{\tau} = [\tau_1 \quad \tau_2]^{\mathrm{T}}$ can be obtained by a PID controller, sliding mode control, feedforward–feedback controller, etc. [23]. In this work, a combined feedforward–feedback control strategy based on a PID controller was applied to control the manipulator, which is expressed as

$$\begin{aligned}
\begin{bmatrix} \tau_1 \\ \tau_2 \end{bmatrix} = \boldsymbol{\tau}_d &+ \begin{bmatrix} P_1 & 0 \\ 0 & P_2 \end{bmatrix}\begin{bmatrix} \theta_{1d} - \theta_1 \\ \theta_{2d} - \theta_2 \end{bmatrix}\\
&+ \begin{bmatrix} D_1 & 0 \\ 0 & D_2 \end{bmatrix}\begin{bmatrix} \dot{\theta}_{1d} - \dot{\theta}_1 \\ \dot{\theta}_{2d} - \dot{\theta}_2 \end{bmatrix}\\
&+ \begin{bmatrix} I_1 & 0 \\ 0 & I_2 \end{bmatrix}\begin{bmatrix} \int_0^t (\theta_{1d} - \theta_1)\mathrm{d}t \\ \int_0^t (\theta_{2d} - \theta_2)\mathrm{d}t \end{bmatrix}
\end{aligned} \tag{19}$$

where P_i, I_i and D_i $(i = 1, 2)$ are the PID controller feedback gains, θ_{id} $(i = 1, 2)$ is the desired angular trajectory, and $\boldsymbol{\tau}_d$ is the feedforward control torque, which

is obtained in the condition of the rigid-body assumption for the manipulator, expressed as,

$$\boldsymbol{\tau}_d = \mathrm{Gdes} + \mathrm{Vdes} + \mathrm{Mdes} * \left[\ddot{\theta}_{1d}\ \ddot{\theta}_{2d}\right]^{\mathrm{T}} \tag{20}$$

where

$$\mathrm{Mdes} = \begin{bmatrix} J_1 + J_2 + m_1\left(\frac{l_1}{2}\right)^2 + m_2\left(\frac{l_2}{2}\right)^2 + m_2 l_1 l_2 \cos\theta_{2d} & J_2 + m_2\left(\frac{l_2}{2}\right)^2 + \frac{1}{2}m_2 l_1 l_2 \cos\theta_{2d} \\ J_2 + m_2\left(\frac{l_2}{2}\right)^2 + \frac{1}{2}m_2 l_1 l_2 \cos\theta_{2d} & J_2 + m_2\left(\frac{l_2}{2}\right)^2 \end{bmatrix} \tag{21}$$

$$\mathrm{Vdes} = \begin{bmatrix} -\frac{1}{2}m_2 l_1 l_2 \sin\theta_{2d}\left(\dot{\theta}_{2d}\dot{\theta}_{1d} + \dot{\theta}_{2d}^2\right) \\ \frac{1}{2}m_2 l_1 l_2 \sin\theta_{2d}\dot{\theta}_{1d}^2 \end{bmatrix} \tag{22}$$

$$\mathrm{Gdes} = \begin{bmatrix} \frac{1}{2}m_1 g l_1 \cos\theta_{1d} + m_2 g\left(l_1 \cos\theta_{1d} + \frac{1}{2}l_2 \cos\left(\theta_{1d} + \theta_{2d}\right)\right) \\ \frac{1}{2}m_2 g l_2 \cos\left(\theta_{1d} + \theta_{2d}\right) \end{bmatrix} \tag{23}$$

where J_1 and J_2 are the moment of inertia of the links OA_i and A_jP_j, respectively, m_1 and m_2 are the mass of the links OA_i and A_jP_j, respectively, l_1 and l_2 are the lengths of the two links, θ_{1d} and θ_{2d} are the designed angles of the links OA_i and A_jP_j, respectively, to track the trajectory, $\dot{\theta}_{1d}$ and $\dot{\theta}_{2d}$ are the designed angular velocities of the two links, and $\ddot{\theta}_{1d}$ and $\ddot{\theta}_{2d}$ are the designed angular accelerations of the two links.

Here, the Lankarani–Nikravesh contact force model and modified Coulomb friction force model are used to construct the generalized contact force. The Lankarani–Nikravesh contact force model [24] is expressed as

$$F_N = K\delta^n\left(1 + \frac{3\left(1 - c_e^2\right)}{4}\frac{\dot{\delta}}{\dot{\delta}^{(-)}}\right) \tag{24}$$

where K is the generalized stiffness constant, c_e is the restitution coefficient, $\dot{\delta}^{(-)}$ is the initial impact velocity, δ and $\dot{\delta}$ are the relative penetration and relative penetration velocity. The value of n depends on the material properties of the impact surfaces, which is set to be 1.5 for most metal contacts. For two spherical surfaces in contact, the generalized stiffness constant is calculated by

$$K = \frac{4}{3\left(h_i + h_j\right)}\left(\frac{R_i R_j}{R_i - R_j}\right)^{\frac{1}{2}} \tag{25}$$

where h_i and h_j are calculated by Eq. (26)

$$h_k = \frac{1 - v_k^2}{E_k} \quad (k = i, j) \tag{26}$$

where E_k and v_k are the Young's modulus and Poisson's ratio, respectively.

The modified Coulomb friction force model [25] is given as

$$F_{\mathrm{T}} = -c_{\mathrm{f}} c_{\mathrm{d}} F_{\mathrm{N}} \frac{\mathbf{v}_{\mathrm{T}}}{v_{\mathrm{T}}} \tag{27}$$

where $\mathbf{v}_{\mathrm{T}}$ and v_{T} are the relative tangential velocity and its scalar component, respectively. c_{f} is the friction coefficient. c_{d} is the dynamic correction coefficient, which is given by

$$c_d = \begin{cases} 0 & \text{if } v_{\mathrm{T}} \le v_0 \\ \frac{v_{\mathrm{T}} - v_0}{v_1 - v_0} & \text{if } v_0 \le v_{\mathrm{T}} \le v_1 \\ 1 & \text{if } v_{\mathrm{T}} \ge v_1 \end{cases} \tag{28}$$

where v_0 and v_1 are the given tolerances for the velocity.

3 Uncertainty analysis of the simplified flexible manipulator

Due to the asymmetry of the material, machining errors and abrasion, uncertainties widely exist in flexible manipulator, such as clearance sizes and Young's moduli of the components, which seriously affect the dynamic performance and kinematic accuracy of the manipulator. In this work, the uncertainties in clearance sizes and Young's moduli are considered, which are described by interval variables and random fields, respectively. Eq. (18) is rewritten as

$$\begin{bmatrix} \mathbf{M} & \tilde{\boldsymbol{\Phi}}_{\mathbf{q}}^{\mathrm{T}} \\ \tilde{\boldsymbol{\Phi}}_{\mathbf{q}} & \mathbf{0} \end{bmatrix}\begin{bmatrix} \ddot{\tilde{\mathbf{q}}} \\ \tilde{\boldsymbol{\lambda}} \end{bmatrix} = \begin{bmatrix} \mathbf{B}\tilde{\boldsymbol{\tau}} - \tilde{\mathbf{F}} + \tilde{\mathbf{F}}_c \\ \tilde{\boldsymbol{\gamma}} - 2\alpha\dot{\tilde{\boldsymbol{\Phi}}} - \beta^2\tilde{\boldsymbol{\Phi}} \end{bmatrix} \tag{29}$$

where the overtilde "$\sim$" expresses the interval variables and random fields. By solving this equation, the dynamic behaviors of the manipulator can be obtained. However, this equation is a differential-algebraic equation containing interval variables and random fields, which is difficult to solve. In this section, a general methodology was presented to solve this problem. Before that, an uncertainty quantization technique was developed to describe the kinematic accuracy of the manipulator obtained by Eq. (29).

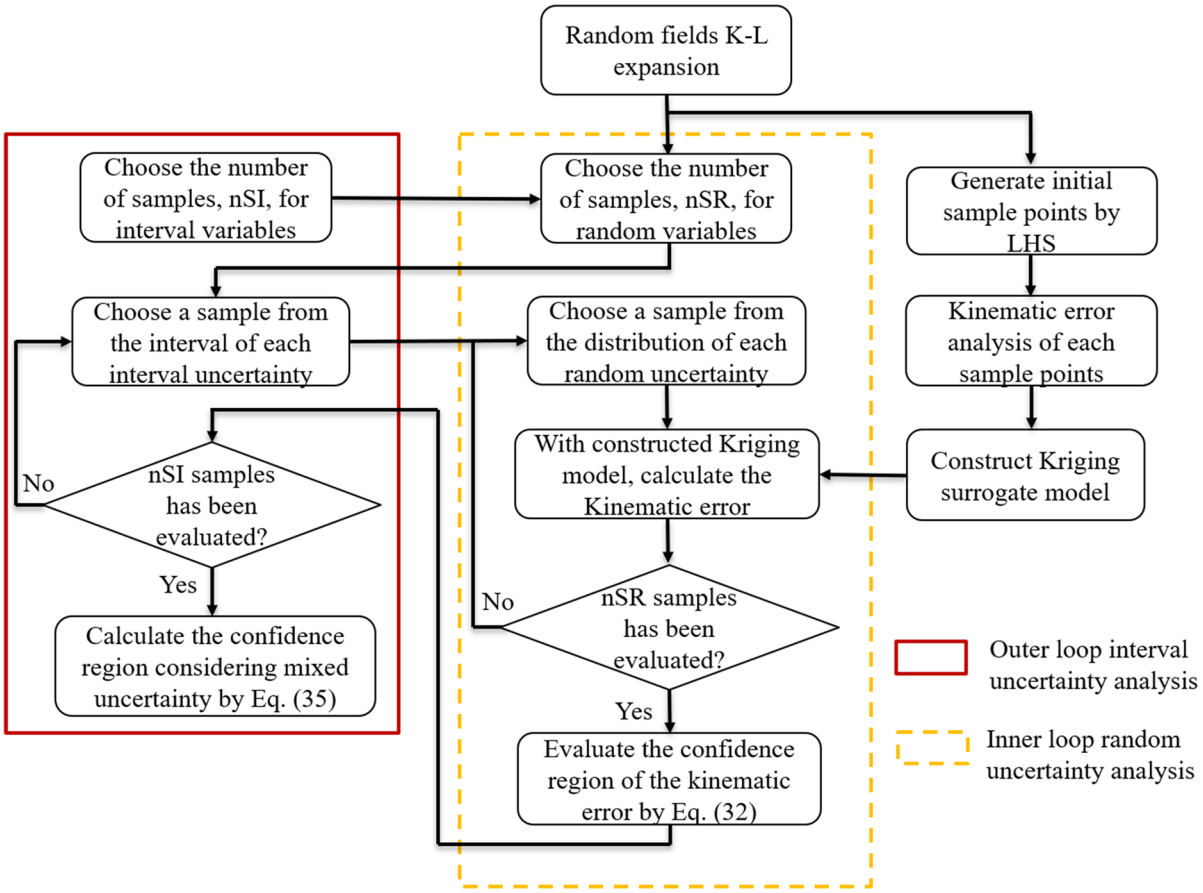

Fig. 3 The time–domain double-loop MCS approach integrating the Karhunen–Loève expansion and Kriging model

3.1 Uncertainty quantization technique of the trajectory accuracy for flexible manipulator with interval variables and random fields

The kinematic error of the flexible manipulator can be expressed as,

$$\tilde{y}(t) = \tilde{\mathbf{q}}_r - \mathbf{q}_d \tag{30}$$

where $\tilde{\mathbf{q}}_r$ and $\mathbf{q}_d$ are the real motion and ideal motion of the manipulator, respectively. Since the real motion of the manipulator is obtained by Eq. (29), the results are influenced by the interval variables and random fields. Thus, Eq. (30) is rewritten as,

$$\tilde{y}(t) = \mathbf{f}(t, \mathbf{a}|\mathbf{e}_M) = \tilde{\mathbf{q}}_r(t, \mathbf{a}|\mathbf{e}_M) - \mathbf{q}_d(t) \tag{31}$$

where $\mathbf{a} = [a_1, \ldots, a_{nA}]$ contains all the nA random fields which is described by mean function $a_0(x)$ and covariance function $C_a(x_1, x_2)$, and $\mathbf{e}_M = \left[e_{M1}, \ldots, e_{M,nM}\right]$ contains all the nM interval variables.

For a fixed $\mathbf{e}_M^k$, the 95% confidence region of the kinematic error for the manipulator with random fields is represented as

$$\begin{aligned} P\left(t|\mathbf{e}_M^k\right) = \Big\{\Big[& y\left(t|\mathbf{e}_M^k\right)_d \; y\left(t|\mathbf{e}_M^k\right)_u\Big] : \\ & \mathrm{Prob}_A\left(\tilde{y}(t) \le y(t)_d, \mathbf{e}_M^k\right) = 2.5\% \text{ and} \\ & \mathrm{Prob}_A(\tilde{y}(t) \le y(t)_u, \mathbf{e}_M^k) = 97.5\% \quad t \in \mathrm{T}\Big\} \end{aligned} \tag{32}$$

where $y\left(t|\mathbf{e}_M^k\right)_d$ and $y\left(t|\mathbf{e}_M^k\right)_u$ denote the lower and upper bounds of the confidence region considering random fields, respectively. $\mathrm{Prob}_A\left(\tilde{y}(t) \le y(t)_d, \mathbf{e}_M^k\right) = 2.5\%$ represents that the probability of $\tilde{y}(t)$ less than $y(t)_d$ is 2.5% with $\mathbf{e}_M$ fixed as indicated, and $\mathrm{Prob}_A\left(\tilde{y}(t) \le y(t)_u, \mathbf{e}_M^k\right) = 97.5\%$ represents that the probability of $\tilde{y}(t)$ less than $y(t)_u$ is 97.5% with $\mathbf{e}_M$ fixed as indicated. $\mathrm{Prob}_A\left(\tilde{y}(t) \le y(t), \mathbf{e}_M^k\right)$ is the probability that $\tilde{y}(t)$ is less than $y(t)$ with $\mathbf{e}_M$ fixed,

and is calculated by Eq. (33).

$$\begin{aligned}&\mathrm{Prob}_A\left(\tilde{y}(t) \le y(t), \mathbf{e}_M^k\right)\\&= \int_\Lambda \delta_y\left[f\left(t, \mathbf{a}|\,\mathbf{e}_M^k\right)\right] d_A\left(\mathbf{a}|\,(a_0, C_a)\right) dA\\&\cong \sum_{i=1}^{nSA} \delta_y\left[f\left(t, \mathbf{a}_i|\,\mathbf{e}_M^k\right)\right]/nSA\end{aligned} \tag{33}$$

where $d_A\left(\mathbf{a}|\,(a_0, C_a)\right)$ is the density function decided by the mean function and covariance function of the random fields. $\mathbf{a}_i$, $i = 1, 2, \ldots, nSA$ is a set of random samples generated from the possible value $\mathbf{a}$ with $\mathbf{e}_M$ fixed. nSA is the number of the random samples. $\underline{\delta}_y$ is calculated by,

$$\delta_y\left[f\left(t, \mathbf{a}|\,\mathbf{e}_M^k\right)\right] = \begin{cases} 1 & \text{if } f\left(t, \mathbf{a}|\,\mathbf{e}_M^k\right) \le y \\ 0 & \text{otherwise} \end{cases} \tag{34}$$

Further taking into account the interval uncertainty, the 95% confidence region of the kinematic error can be expressed as

$$\begin{aligned}\Psi(t) = \big\{&\left[y(t)_d \;\; y(t)_u\right] : y(t)_d\\&= \min\left(y(t|\,\mathbf{e}_M)_d\right) \text{ and } y(t)_u\\&= \max\left(y(t|\,\mathbf{e}_M)_u\right) \quad t \in \mathrm{T} \text{ and } \quad \mathbf{e}_M \in \Xi\big\}\end{aligned} \tag{35}$$

where $y(t)_d$ and $y(t)_u$ denote the lower and upper bounds of the confidence region considering random fields and interval variables, respectively. Ξ contains all possible values for $\mathbf{e}_M$.

3.2 The time–domain double-loop MCS approach integrating the Karhunen–Loève expansion and Kriging model

To obtain the 95% confidence region of the kinematic error for the manipulator, a general methodology was developed. Considering the inefficiency of the uncertainty analysis, a time–domain double-loop MCS approach integrating the Karhunen–Loève expansion and Kriging model (TDMSC) is presented in this section. The main procedures of the approach are shown in Fig. 3 with the following steps.

(1) Transform the random field $\mathbf{a} = [a_1, \ldots, a_{nA}]$ into uncorrelated random variables $\boldsymbol{\xi} = \left[\left[\xi_1^1, \ldots, \xi_1^{m1}\right], \ldots, \left[\xi_{nA}^1, \ldots, \xi_{nA}^{mn}\right]\right]$ by the Karhunen–Loève expansion method.

In the Karhunen–Loève expansion method [26,27], a random field, $H(\mathbf{x}, \theta)$, can be expanded as the following form,

$$H(\mathbf{x}, \theta) = \mu(\mathbf{x}) + \sum_{i=1}^{\infty} \sqrt{\lambda_i}\varphi_i(\mathbf{x})\xi_i(\theta) \tag{36}$$

where $\mu(\mathbf{x})$ is the mean function of the random field, $\xi_i(\theta)$ $(i = 1, 2, \ldots)$ is the standard uncorrelated random variables, $\varphi_i(\mathbf{x})$ and λ_i are the eigenfunctions and eigenvalues of the covariance function $\mathrm{Cov}\left(\mathbf{x}, \mathbf{x}'\right)$, respectively.

(2) Generate sample points by using the Latin hypercube sample (LHS) method.
(3) Predict the kinematic error of the manipulator of each sample point by using the generalized-α method.
(4) With the sample points and corresponding kinematic error, construct a surrogate model by the Kriging method [28].
(5) Choose the number of samples, nSI, for interval variables.
(6) Choose the number of samples, nSR, for random variables obtained by Step 1.
(7) Choose a sample from the interval of each interval uncertainty by the LHS method.
(8) Choose a sample from the distribution of each random uncertainty based on the MCS approach.
(9) With the constructed Kriging model, calculate the kinematic error of the manipulator by using the complete array of the sample points.
(10) Test whether all nSR random sample points have been predicted. If Yes, go to Step 11; if No, return to Step 8.
(11) Evaluate the confidence region of the kinematic error of the manipulator by Eq. (32).
(12) Test whether all nSI interval sample points have been predicted. If Yes, go to Step 13; if No, return to Step 7.

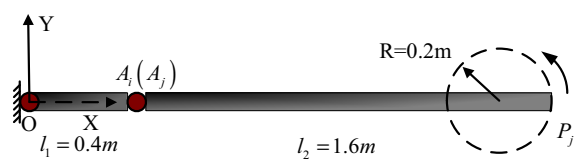

Fig. 4 Circle trajectory tracking of the two-link flexible manipulator

Table 1 Parameters for the dynamic analysis of the two-link flexible manipulator

Journal radius for joints O and A	10.0 mm	Friction coefficient for joints O and A	0.1
Restitution coefficient for joints O and A	0.9	Young's modulus for joints O and A	207 GPa
Poisson's ratio for joints O and A	0.3	Integration step size	0.00001 s
Baumgarte-α, β	250	Integration tolerance	0.000001

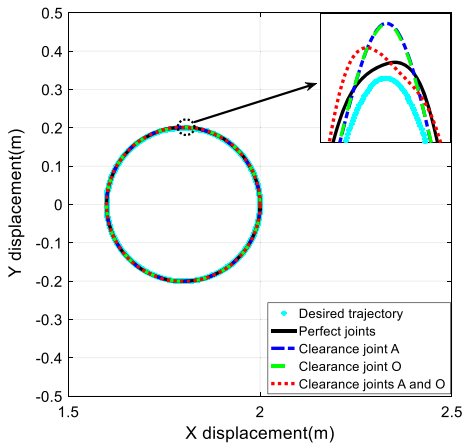

Fig. 5 The tip trajectory of the manipulator for different number of clearance joints

(13) Calculate the confidence region of the kinematic error of the manipulator with hybrid uncertainties by Eq. (35).

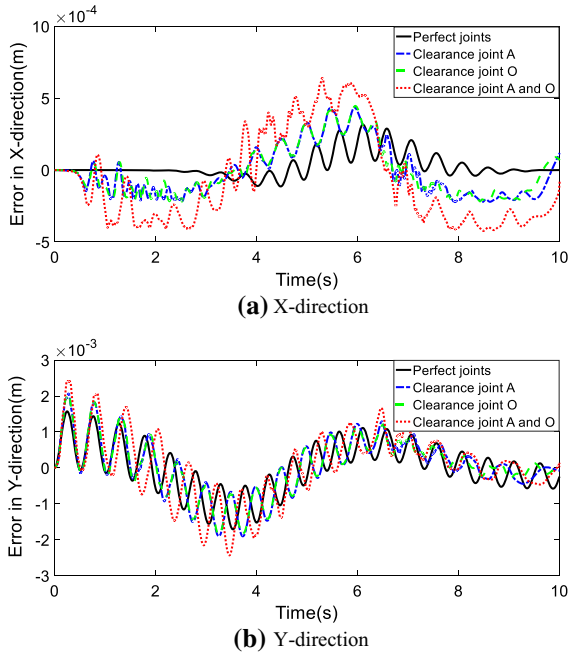

Fig. 6 Trajectory errors of the manipulator in the X-direction and Y-direction for different number of clearance joints

4 Results and discussion

The two-link flexible manipulator with clearance joints was controlled to track a circle trajectory, as shown in Fig. 4, with the designed angular velocity as follows

$$\omega = -\frac{6\pi}{500}\left(t^2 - 10t\right) \tag{37}$$

The links OA_i and A_jP_j are made of aluminum alloy. The initial lengths of links OA_i and A_jP_j are 0.4 m and 1.6 m, respectively. Links OA_i and A_jP_j were discretized by four and ten elements, respectively. The cross-sectional area, the second moment of area, the Young's modulus and the mass density of the links OA_i and A_jP_j are 1.0×10^{-4} m^2, 8.333×10^{-10} m^4, 68 GPa and 2698.9 kg/m^3, respectively. In this work, a combined feedforward–feedback control strategy based on a PID controller is applied to control the tip trajectory of the manipulator. The proportional, derivative and integrative gains of the PID controllers for all numerically simulated cases below are 2000, 30 and 30, respectively. The parameters for the dynamic analysis of the manipulator are shown in Table 1.

To investigate the influences of the number of clearance joints on the dynamic behaviors and kinematic accuracy of the two-link flexible manipulator, the manipulator is simulated for four different cases: (1) Joints O and A are perfect joints (Perfect joints), (2) Joint O is a perfect joint, while joint A is an imperfect joint with 0.2 mm clearance (Clearance joint A), (3) Joint A is a perfect joint, while joint O is an imperfect joint with 0.2 mm clearance (Clearance joint O), (4) Joints O and A are imperfect joints with 0.2 mm clearance (Clearance joints A and O). Figure 5 shows the

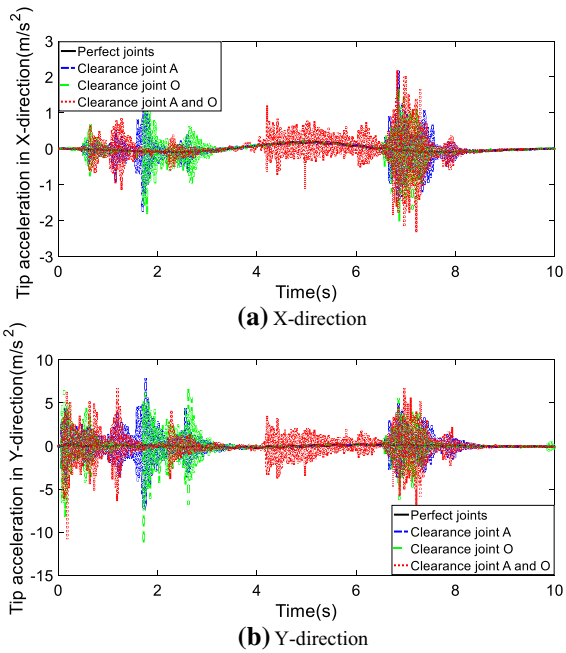

Fig. 7 Tip acceleration of the manipulator in the X-direction and Y-direction for different number of clearance joints

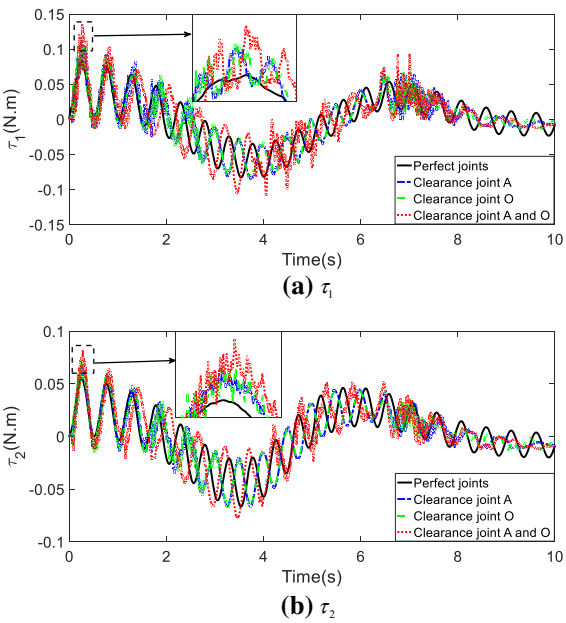

Fig. 8 Control torques of the manipulator for different number of clearance joints

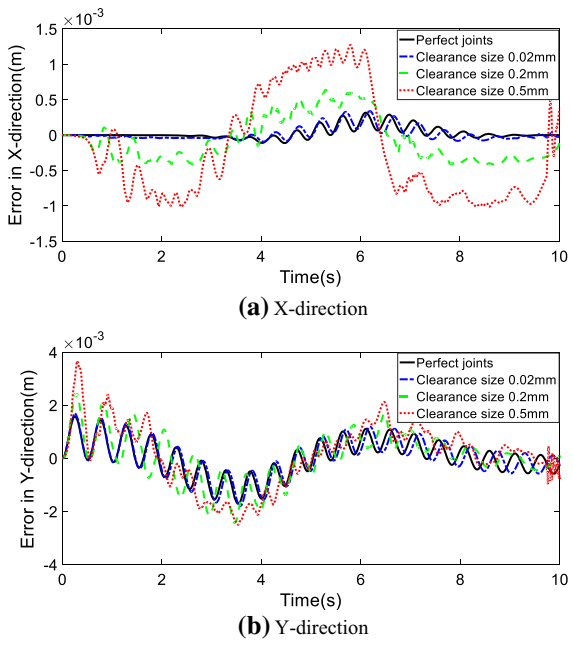

Fig. 9 Trajectory errors of the manipulator in the X-direction and Y-direction for different clearance sizes

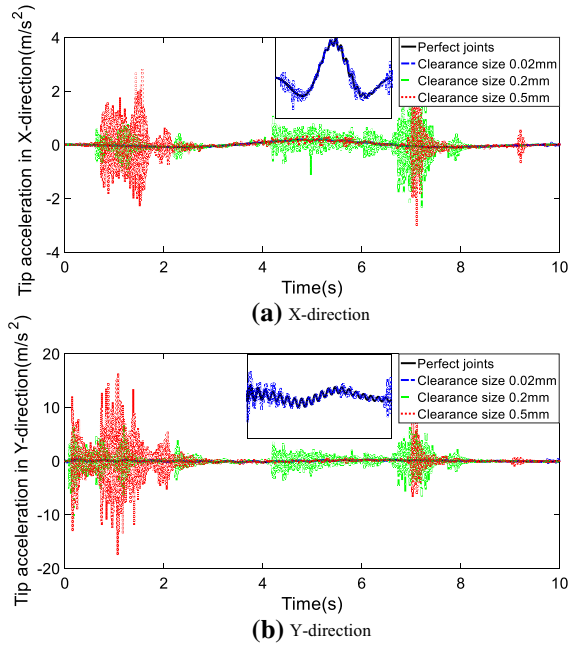

Fig. 10 Tip acceleration of the manipulator in the X-direction and Y-direction for different clearance sizes

tip trajectory of the manipulator for different number of clearance joints. It is observed that joint clearance can affect the kinematic accuracy of the manipulator. Figure 6a, b shows the trajectory errors of the manipulator in the X-direction and Y-direction for different number of clearance joints, respectively. It is seen that the

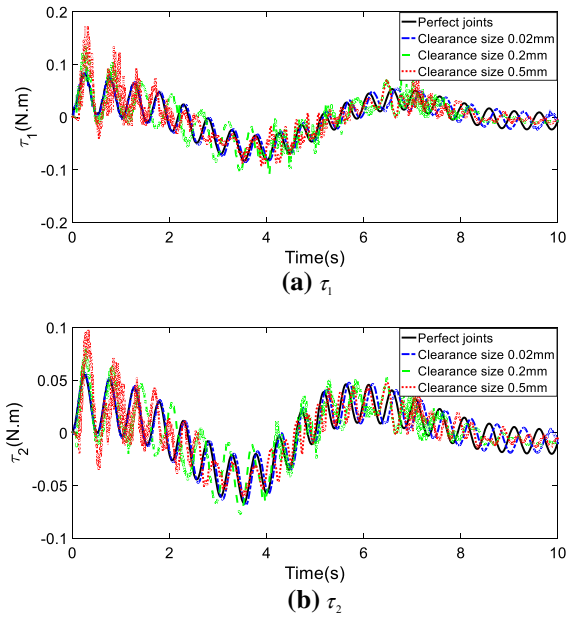

Fig. 11 Control torques of the manipulator for different clearance sizes

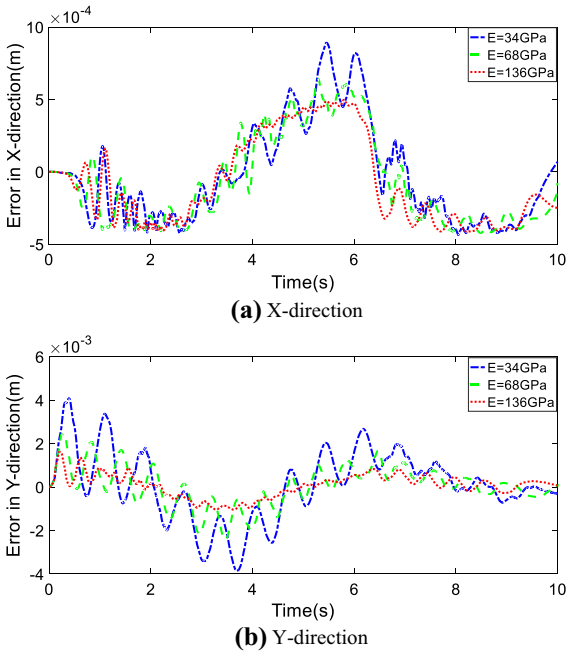

Fig. 12 Trajectory errors of the manipulator in the X-direction and Y-direction for different Young's moduli

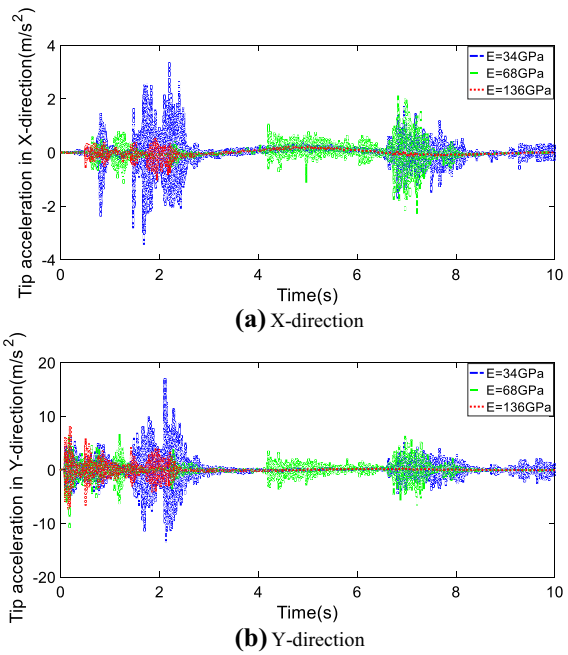

Fig. 13 Tip acceleration of the manipulator in the X-direction and Y-direction for different Young's moduli

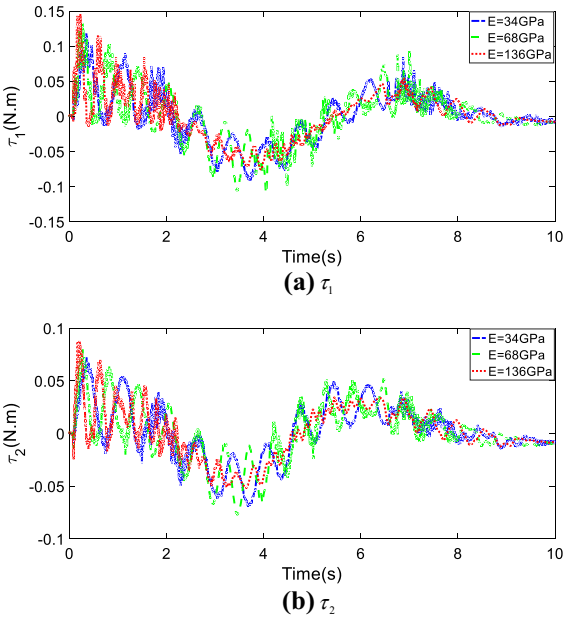

Fig. 14 Control torques of the manipulator for different Young's moduli

maximum trajectory error of the manipulator with two clearance joints is larger than that with single clearance joint. Comparing case 2 and case 3, it indicates that the position of clearance can affect the trajectory errors of the manipulator. Figure 7a, b shows the tip acceleration of the manipulator in the X-direction and Y-direction. It

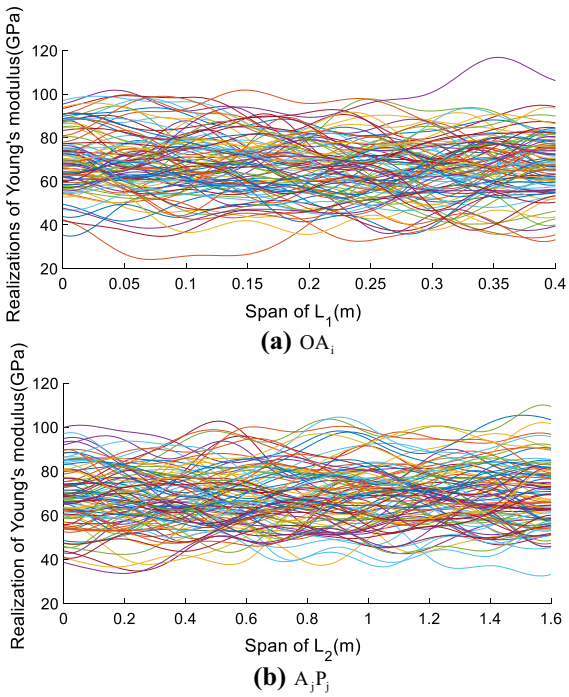

Fig. 15 Illustrations of random fields

Table 2 Four cases with different uncertainty situations

Parameter	Case1	Case2	Case3	Case4
Clearance size (mm)	[0.2, 0.3]	[0.2, 0.3]	0.25	0.25
Young's modulus (GPa)	68	$E(x,\theta)$	$E(x,\theta)$	68

indicates that joint clearance leads to high acceleration peaks. There are more pronounced peaks as the number of clearance joints increases. The peak values are showed in different times between case 2 (Clearance joint A) and case 3 (Clearance joint O). Form Fig. 8a, b, it is seen that the maximum control torques are larger as the number of clearance joints increases. In addition, the control torques when the clearance at joint O have higher peaks as compared to that when the clearance at joint A.

To further study the influences of the clearance on the dynamic behaviors and kinematic accuracy of the manipulator, the clearance size for the manipulator with two clearance joints was selected as 0.02 mm, 0.2 mm and 0.5 mm, respectively. Figure 9a, b shows that the trajectory errors of the manipulator with perfect joints are close to the results for clearance size 0.02 mm in 0–4 s. However, there is obvious difference in 6–10 s. The peak values of the two curves are close. The difference is mainly reflected in the movement of the phase. The effect of the clearance on the kinematic accuracy of the manipulator is obvious when the clearance size is 0.2 mm or 0.5 mm. The effects are reflected in not only phase but also peak. The maximum trajectory errors are larger as the clearance size increases. When the clearance size is 0.02 mm, the vibration of the trajectory errors is low-frequency vibration. However, when the clearance size is 0.2 mm or 0.5 mm, due to the violent collision of clearance, the trajectory errors will appear as high-frequency vibration. Figure 10a, b shows the tip acceleration of the manipulator in the *X*-direction and *Y*-direction. It indicates that the tip acceleration of the manipulator has obviously shaken, and the amplitude is increased when joint clearance is considered. Figure 11a, b indicates that the maximum control torques are larger as the clearance size increases, and large clearance size leads to more pronounced peaks.

The Young's modulus of the manipulator with two clearance joints was assumed to be 34 GPa, 68 GPa and 136 GPa, respectively, while the clearance size was 0.2 mm. The trajectory errors of the manipulator for different Young's moduli are shown in Fig. 12. It is obvious that the trajectory errors of the manipulator are smaller as the Young's modulus increases. As shown in Fig. 13, there are less pronounced peaks for the tip accelerations of the manipulator as the Young's modulus increase. Figure 14 shows the control torques of the manipulator. It indicates that the maximum control torques are larger as the Young's modulus increases.

Considering the influence of the clearance and the flexibility of the components on the dynamic performance and kinematic accuracy of the manipulator, uncertainties of these two parameters were considered. In this work, interval variables and random fields were used to represent the uncertainties of the clearance sizes and Young's moduli of the flexible parts, respectively. The interval clearance is given by $c \in [0.2, 0.3]$ mm. Young's modulus of the flexible parts is the stationary Gaussian random field of the form,

$$E(x,\theta) = \bar{E}\,(1 + a(x,\theta)) \tag{38}$$

where $\bar{E} = 68\text{GPa}$. $a(x,\theta)$ is the stationary Gaussian field with zero mean, and its covariance function is $C_a(x_1, x_2) = \sigma_a^2 e^{(|x_1-x_2|)/\mu_a}$. σ_a and μ_a are the standard deviation and correlation length, respectively. For the links OA_i and A_jP_j, the correlation lengths are $l_1/2$ and $l_2/2$, respectively, with the same standard devia-

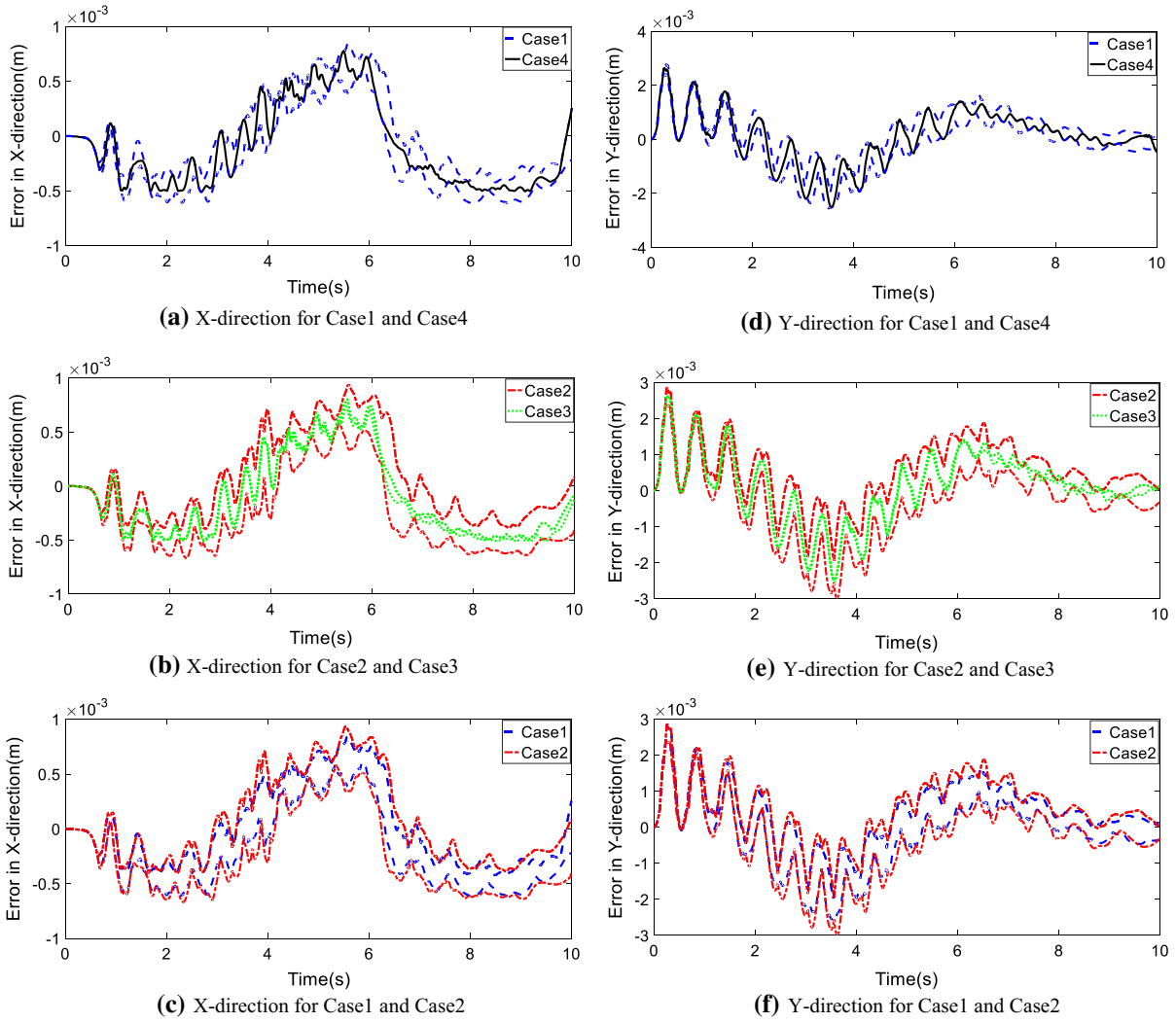

Fig. 16 Trajectory errors of the manipulator in the X-direction and Y-direction for different uncertainty situations

tion ($\sigma_a = 0.2$). The illustrations of the random field are presented in Fig. 15.

Four cases with different uncertainty situations, as shown in Table 2, are simulated. The confidence regions of the trajectory errors, tip accelerations and control torques of the manipulator with different uncertainty situations are given in Figs. 16, 17 and 18. From Fig. 16, it is seen that there are obvious differences between the trajectory errors of the manipulator with deterministic parameters and uncertain parameters. And the differences become larger when time increases. The trajectory errors of the manipulator with deterministic parameters are contained in those with interval uncertainty. The trajectory errors with hybrid uncertainties are larger than those with interval uncertainty or those with random uncertainty. The comparison of tip accelerations among the deterministic model, random uncertain model, interval uncertain model and hybrid uncertain model, as shown in Fig. 17, indicates that the uncertainty significantly affects the tip accelerations of the manipulator. The tip accelerations of the manipulator with deterministic parameters are contained in those with interval uncertainty, while the results considering random fields are contained in those considering hybrid uncertainties. However, due to large pronounced peaks, the tip accelerations of the manipulator with inter-

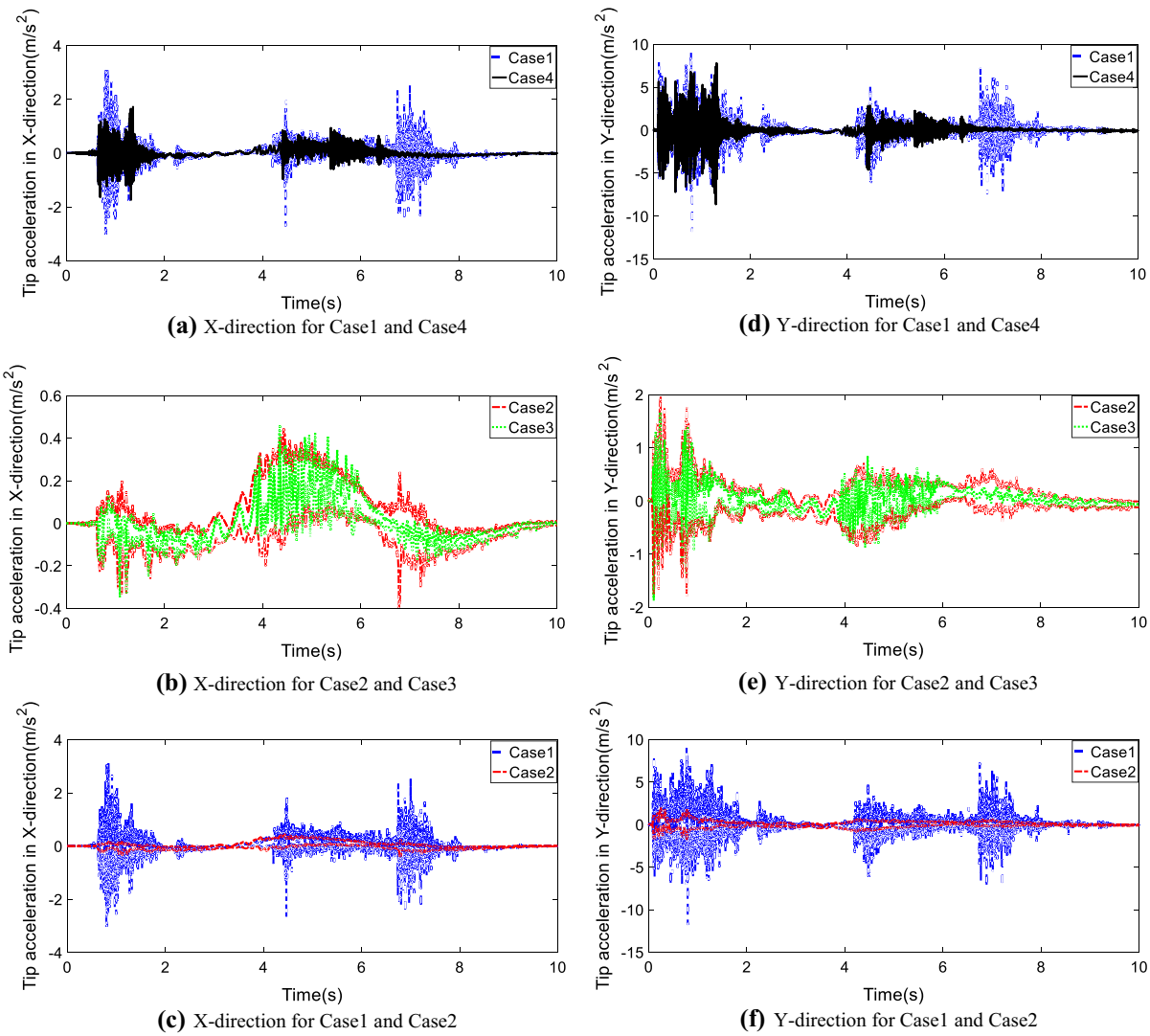

Fig. 17 Tip acceleration of the manipulator in the X-direction and Y-direction for different uncertainty situations

val uncertainty are not contained in those with hybrid uncertainties. Comparing with the interval method, the tip accelerations of the manipulator obtained by the proposed method have less pronounced peaks. Figure 18 indicates that uncertainty significantly affects the control torques of the manipulator, while the effect is more serious when the hybrid uncertainties are considered.

5 Conclusions

The current work presented a computational methodology for kinematic accuracy and dynamic analysis of a simplified flexible manipulator with multiple revolute clearance joints and hybrid uncertainties, considering the inhomogeneous distribution of the material properties in space domain. The Lankarani–Nikravesh contact force model was employed to construct the clearance joint, while a combined feedforward–feedback control strategy based on a PID controller was applied to control the manipulator. Moreover, interval uncertainty and random field were applied to represent the uncertainty of the clearance size and material properties, respectively. Due to the complexity of the dynamics model of the manipulator and the challenges to

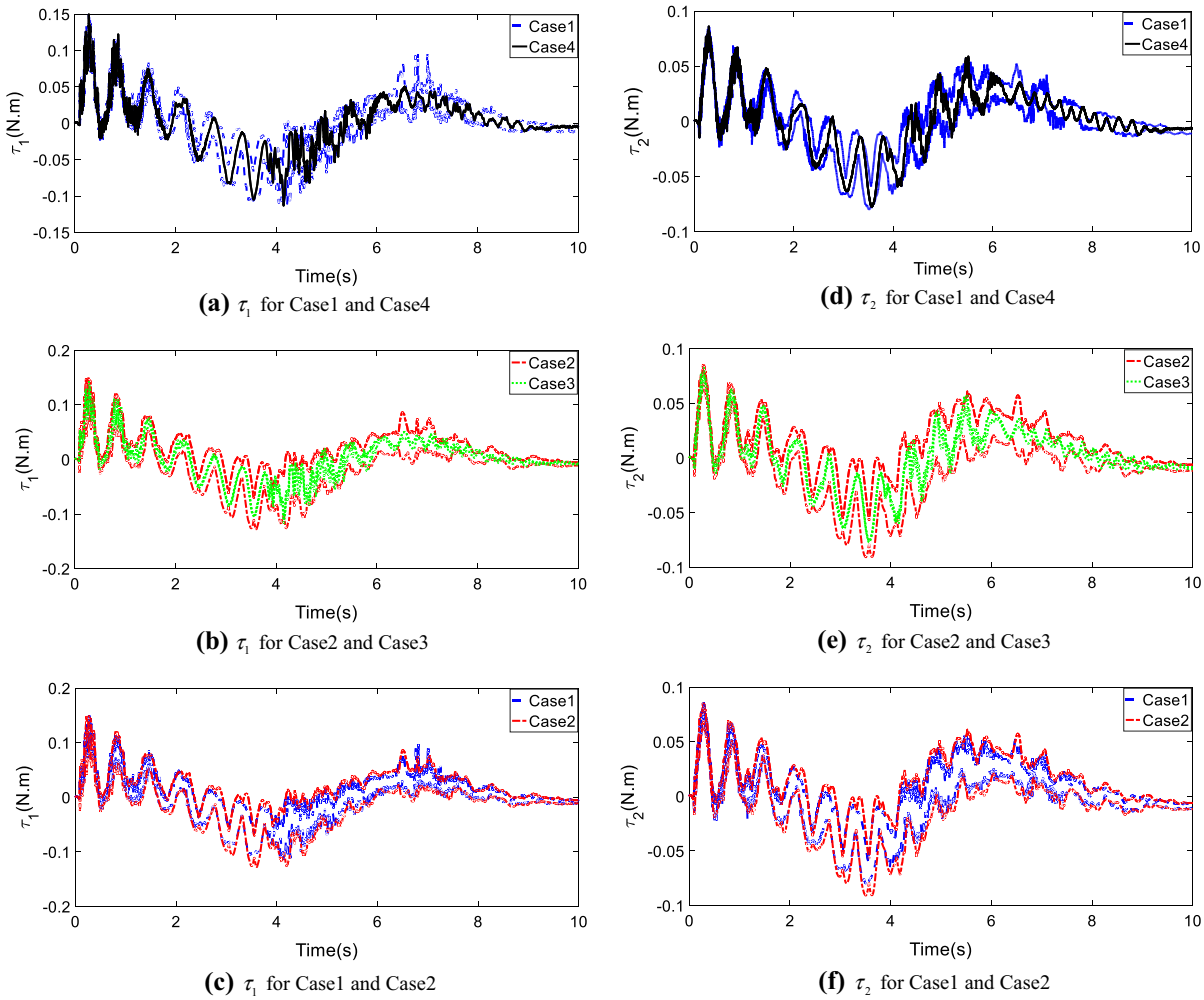

Fig. 18 Control torques of the manipulator for different uncertainty situations

solve the problem, a time–domain double-loop MCS approach integrating the Karhunen–Loève expansion and Kriging model was developed, which is a general method for dynamic analysis of a flexible manipulator with interval uncertainty and random fields. The simulation results of a two-link flexible manipulator with clearance joints, controlled to track a circle trajectory, led to the following observations. The joint clearance significantly affected the dynamic behaviors, kinematic accuracy and control torques of the manipulator. And the effect was more serious as the number of clearance joints increased. Meanwhile, the maximum control torques are larger as the clearance size increased. The flexibility of the components has obvious influences on the dynamic behaviors, kinematic accuracy and control torques of the manipulator. The maximum control torques are also larger as the Young's modulus increased. Uncertainty reduced the kinematic accuracy of the manipulator. Hybrid uncertainties resulted in worse kinematic accuracy and more complex dynamic behaviors. Uncertainty also can significantly affect the control torques of the manipulator, while the effect is more serious when the hybrid uncertainties are considered.

Acknowledgements This work was supported by Chongqing Research Program of Basic Research and Frontier Technology (Grant No. cstc2016jcyjA0378), Fundamental Research Funds for Central Universities (Grant No. 2018CDXYHK0016), National Natural Science Foundation of China (Grant No.

51505398, 11702131), NSAF (Grant No. U1530122) and Aeronautical Science Foundation of China (Grant No. 20150968003).

Compliance with ethical standards

Conflict of interest The authors declare that they have no conflict of interest.

References

1. Tian, Q., Flores, P., Lankarani, H.M.: A comprehensive survey of the analytical, numerical and experimental methodologies for dynamics of multibody mechanical systems with clearance or imperfect joints. Mech. Mach. Theory **122**, 1–57 (2018)
2. Erkaya, S.: Investigation of joint clearance effects on welding robot manipulators. Robot. Comput. Integr. Manuf. **28**, 449–457 (2012)
3. Varedi, S.M., Daniali, H.M., Farajtabar, M.: The effects of joint clearance on the dynamics of the 3RRR planar parallel manipulator. Robotica **35**, 1223–1242 (2017)
4. Varedi, S.M., Daniali, H.M., Farajtabar, M., Fathi, B., Shafiee-Ashtiani, M.: Reducing the undesirable effects of joints clearance on the behavior of the planar 3-RRR parallel manipulators. Nonlinear Dyn. **86**, 1007–1022 (2016)
5. Bai, Z., Sun, Y.: A study on dynamics of planar multibody mechanical systems with multiple revolute clearance joints. Eur. J. Mech. Solids **60**, 95–111 (2016)
6. Ma, J., Qian, L.: Modeling and simulation of planar multibody systems considering multiple revolute clearance joints. Nonlinear Dyn. **90**, 1907–1940 (2017)
7. Zhang, H., Zhang, X., Zhang, X., Mo, J.: Dynamic analysis of a 3-PRR parallel mechanism by considering joint clearances. Nonlinear Dyn. **90**, 405–423 (2017)
8. Abdallah, M.A.B., Khemili, I., Aifaoui, N.: Numerical investigation of a flexible slider-crank mechanism with multijoints with clearance. Multibody Syst. Dyn. **38**, 173–199 (2016)
9. Li, H., Yu, Z., Guo, S., Cai, G.: Investigation of joint clearances in a large-scale flexible solar array system, Multibody Syst. Dyn. **44**, 277–292 (2018)
10. Tian, Q., Liu, C., Machado, M., Flores, P.: A new model for dry and lubricated cylindrical joints with clearance in spatial flexible multibody systems. Nonlinear Dyn. **64**, 25–47 (2011)
11. Helton, J.C., Johnson, J.D.: Quantification of margins and uncertainties: alternative representations of epistemic uncertainty. Reliab. Eng. Syst. Saf. **96**, 1034–1052 (2011)
12. Helton, J.C.: Quantification of margins and uncertainties: conceptual and computational basis. Reliab. Eng. Syst. Saf. **96**, 976–1013 (2011)
13. Chaker, A., Mlika, A., Laribi, M.A., Romdhane, L., Zeghloul, S.: Clearance and manufacturing errors' effects on the accuracy of the 3-RCC spherical parallel manipulator. Eur. J. Mech. Solids **37**, 86–95 (2013)
14. Pandey, M.D., Zhang, X.: System reliability analysis of the robotic manipulator with random joint clearances. Mech. Mach. Theory **58**, 137–152 (2012)
15. Li, J., Huang, H., Yan, S., Yang, Y.: Kinematic accuracy and dynamic performance of a simple planar space deployable mechanism with joint clearance considering parameter uncertainty. Acta Astronaut. **136**, 34–45 (2017)
16. Sun, D.: Tracking accuracy analysis of a planar flexible manipulator with lubricated joint and interval uncertainty. J. Comput. Nonlinear Dyn. **11**, 051024 (2016)
17. Yan, S., Guo, P.: Kinematic accuracy analysis of flexible mechanisms with uncertain link lengths and joint clearances. Proc. Inst. Mech. Eng. Part C J. Eng. Mech. Eng. Sci. **225**, 1973–1983 (2011)
18. Wang, Z., Tian, Q., Hu, H.: Dynamics of flexible multibody systems with hybrid uncertain parameters. Mech. Mach. Theory **121**, 128–147 (2018)
19. Sun, D., Chen, G.: Kinematic accuracy analysis of planar mechanisms with clearance involving random and epistemic uncertainty. Eur. J. Mech. Solids **58**, 256–261 (2016)
20. Wu, J., Luo, Z., Zhang, N., Zhang, Y.: Dynamic computation of flexible multibody system with uncertain material properties. Nonlinear Dyn. **85**, 1231–1254 (2016)
21. Wu, J., Luo, Z., Zhang, N., Zhang, Y., Walker, P.D.: Uncertain dynamic analysis for rigid-flexible mechanisms with random geometry and material properties. Mech. Syst. Signal Process. **85**, 487–511 (2017)
22. Escalona, J.L., Hussien, H.A., Shabana, A.A.: Application of the absolute nodal coordinate formulation to multibody system dynamics. J. Sound Vib. **214**, 833–851 (1998)
23. Dwivedy, S.K., Eberhard, P.: Dynamic analysis of flexible manipulators, a literature review. Mech. Mach. Theory **41**, 749–777 (2006)
24. Lankarani, H.M.: A contact force model with hysteresis damping for impact analysis of multibody systems. J. Mech. Des. **112**, 369–376 (1990)
25. Ambrósio, J.A.C.: Impact of Rigid and Flexible Multibody Systems: Deformation Description and Contact Models, Virtual Nonlinear Multibody Systems, pp. 57–81. Springer, Dordrecht (2003)
26. Betz, W., Papaioannou, I., Straub, D.: Numerical methods for the discretization of random fields by means of the Karhunen–Loève expansion. Comput. Methods Appl. Mech. Eng. **271**, 109–129 (2014)
27. Adhikari, S., Friswell, M.I.: Distributed parameter model updating using the Karhunen–Loève expansion. Mech. Syst. Signal Process. **24**, 326–339 (2010)
28. Zhang, Z., Xu, L., Flores, P., Lankarani, H.M.: A Kriging model for the dynamics of mechanical systems with revolute joint clearances. J. Comput. Nonlinear Dyn. **9**, 031013 (2014)